Supplement of The Cryosphere, 20, 3913–3932, 2026
https://doi.org/10.5194/tc-20-3913-2026-supplement

The Cryosphere
Open Access

Supplement of

Bayesian inversion of satellite altimetry for Arctic sea ice and snow thickness

Elie René-Bazin et al.

Correspondence to: Elie René-Bazin (elie.rene-bazin@ens-lyon.fr)

1 Details on data location

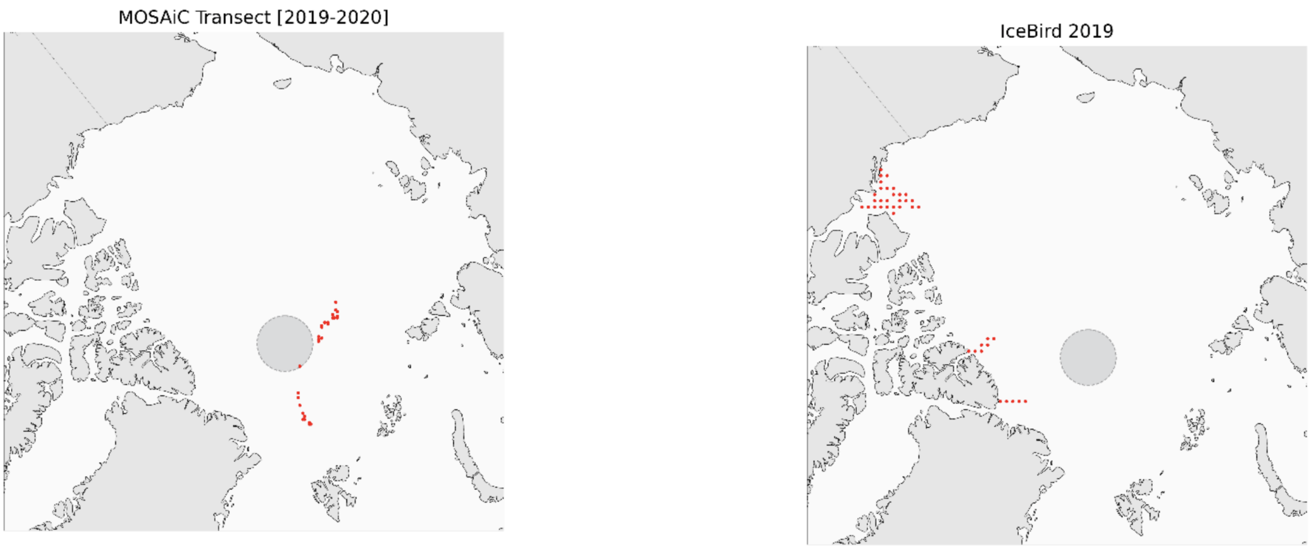

Figure S1. (left) MOSAiC tracks for Winter 2019-2020 (right) IceBird tracks for 2019/04. Figure taken from the Polar+ project (Hendricks et al (2025), Polar+ Snow on Sea Ice Product Validation Report document, https://www.cpom.ucl.ac.uk/snow-on-sea-ice/public-docs.html)

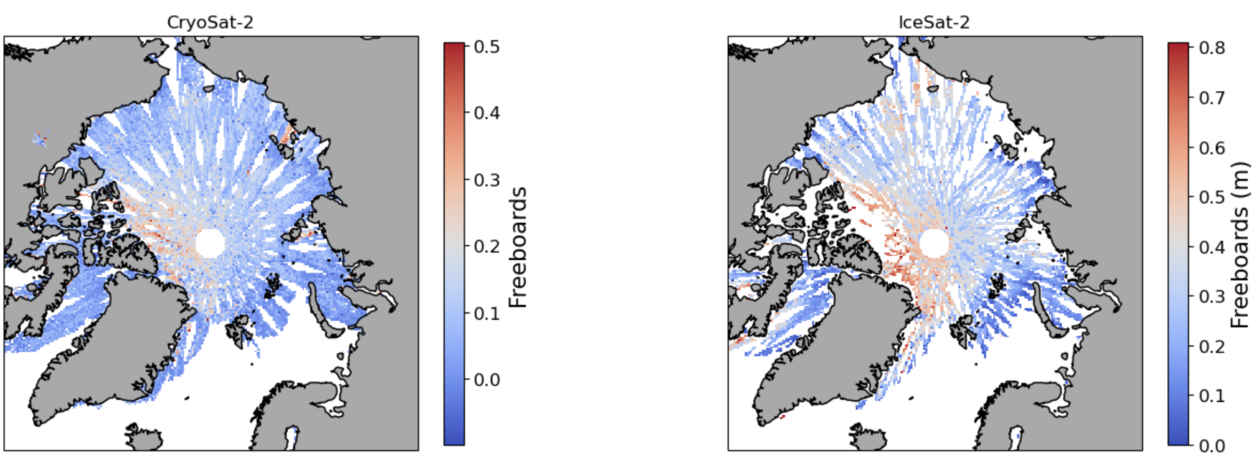

Figure S2. Example of input for April 2019 with the CS-IS satellite combination. The input is composed of daily along-track freeboard data binned on a 25 km^2 EASE2 grid, for each satellite.

2 Example of input uncertainties

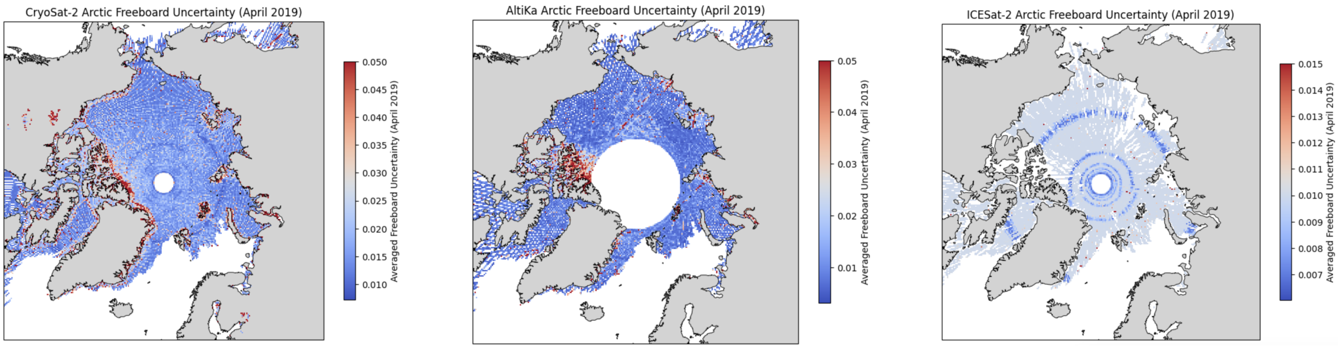

Figure S3. Input uncertainties used for 2019/04.

3 Example of computed standard deviations

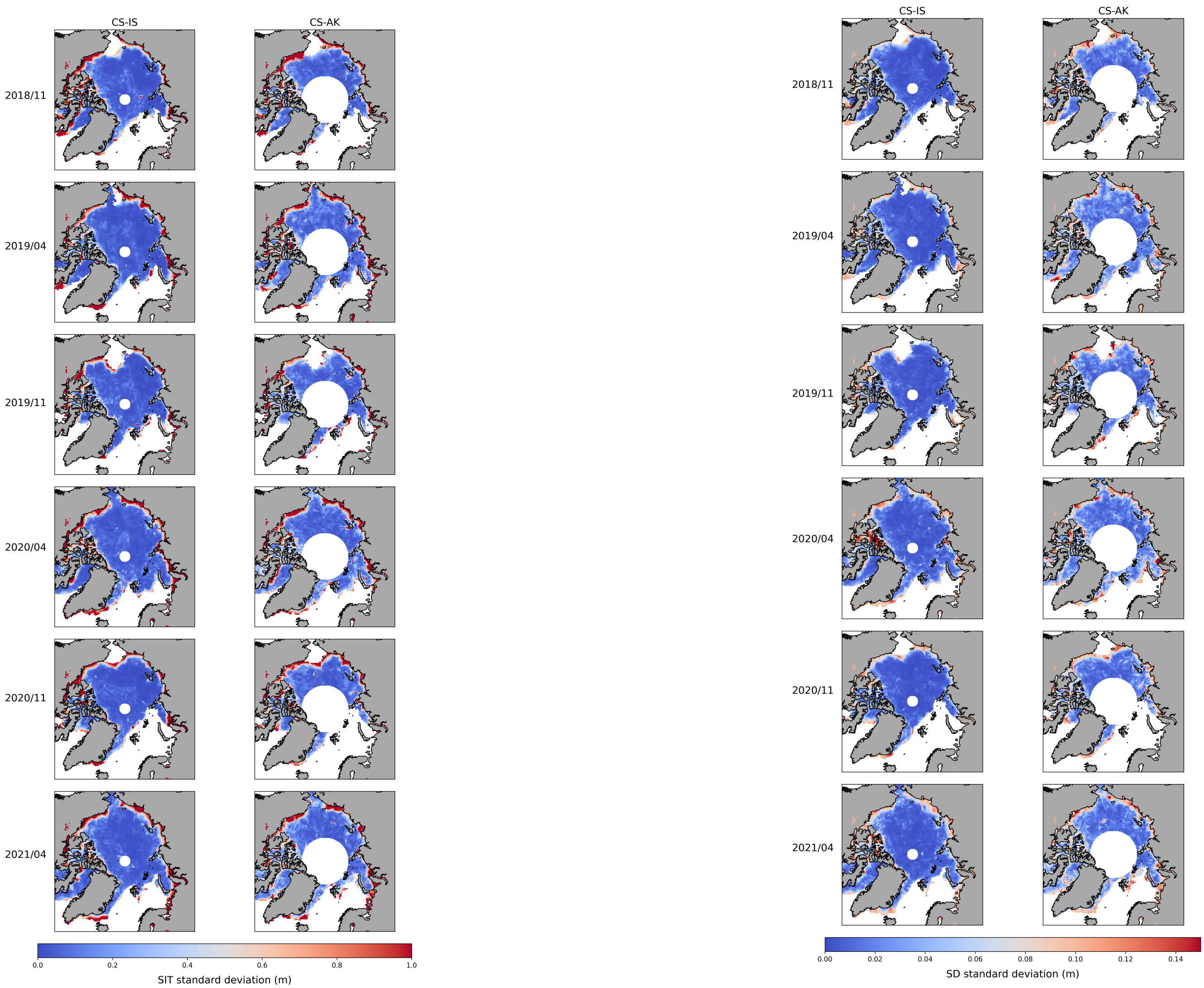

Figure S4. Standard deviations for (left) SIT and (right) SD, computed following the inversion for CS-IS-2p and CS-AK-2p.

4 Inversion for the bias factors in addition of SIT and SD

We chose the following intervals for the prior distributions:

- α_{cs}: $[-0.5, 1.5]$ (for CS-IS-3p) or $[0.5, 1.5]$ (for CS-IS-4p)
- α_{is}: $[-0.5, 0.5]$

We choose wide intervals for α_{cs} and α_{is} to allow a large degree of freedom to the method (even if a negative bias factor doesn't have a physical meaning). Using these defined prior distributions $P(m_{\alpha_{cs}})$ and $P(m_{\alpha_{is}})$, the method allow to computes maps for each bias factor.

In Figure S5, we find the results of the inversion for CS-IS-3p for winter 2020-2021 (every month from November to April). We find that both SD and SIT are increasing from November to April. We retrieve the expected spatial patterns for ice and snow (high SIT (2 - 4 m) and SD (> 0.4 m) north of Greenland). We find an asymmetry between West and East of Baffin Bay, with a higher SD on the West part of the bay, especially for April. On the maps for SIT, this asymmetry is less obvious, even if it is distinguishable for April. Looking at the maps for the bias factor α_{cs}, the general patterns are close to no bias (α_{cs} = 1) over MYI north of Greenland and Canada, and over FYI in the Arctic Ocean's marginal seas, but only some bias (α_{cs} between 0.5 and 0.75) over the second year ice in the Central Arctic. From November to April, the bias factor maps are very similar. Some changes can be seen over the Canadian Archipelago and more generally on the borders of the Arctic Ocean.

There are some similarities when comparing the maps for α_{cs} and the results for SIT and SD. Especially for April, the bias factor is important around Wrangel Island. In this same area, SIT is higher (close to 3 m). Similarly, on the north of Greenland where $\alpha_{cs} \simeq 1$, the SIT is important (around 4.5 m in some places) but here the SD is also important (even if we find a thinner ice close to the Canadian Archipelago).

In the map for November, we can see that the spatial patterns of the snow and the values obtained are quite similar to the one of the AMSR2 product and also to the result with CS-IS-2p. However, the map for April is very different from the AMSR2 product with a higher SD all over the Arctic Ocean (> 0.4 m). Over Baffin Bay, we can observe a important asymmetry between West and East, with an higher SD on the West part of the Bay, especially for 2019/04. On the maps for SIT, we don't observe this asymmetry. This is similar to the maps obtained using CS-IS-2p for which we don't observe significant asymmetry for the SIT but for the SD. However, this asymmetry for the SIT is noted in other studies. This could be a problem of spatial resolution and smoothing of the solution by the method.

As detailed previously, the boundaries for the prior distribution on this bias factor are [-0.5;1.5], with the range of values inverted for between 0.5 and 1.2 approximately. This suggests that the algorithm, using a prior with a great degree of freedom, is capable of retrieving values for α_{cs} that are similar to those in the literature.

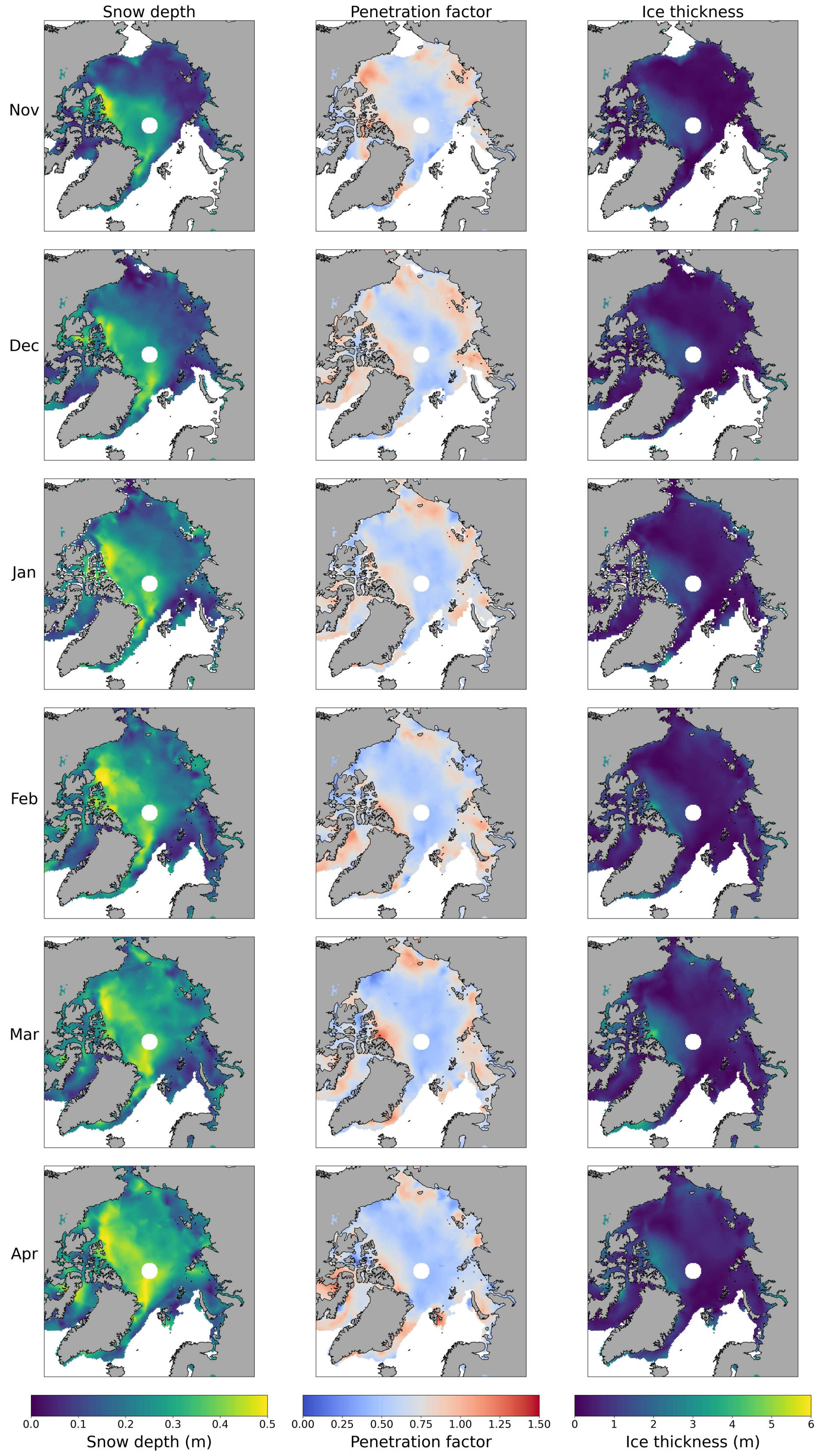

Figure S5. Inverse solution for CS-IS-3p for winter 2020-2021 (November to April). The inversion is performed for the (left column) SD, (middle column) bias factor of CS and (right column) SIT. We assume $\alpha_{is} = 0$.

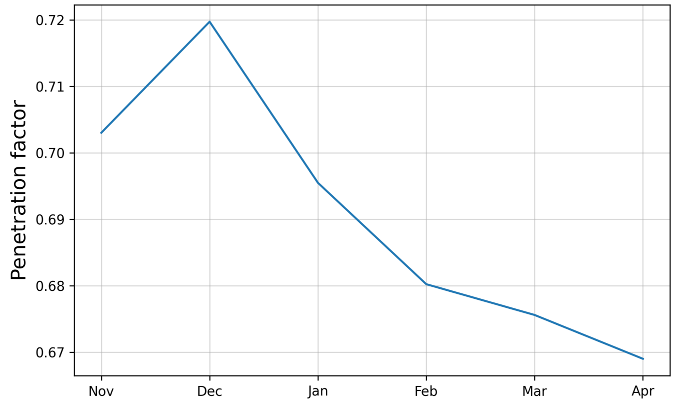

Figure S6. Pan-Arctic average of α_{cs} for Winter 2020-2021 (see Figure S5)

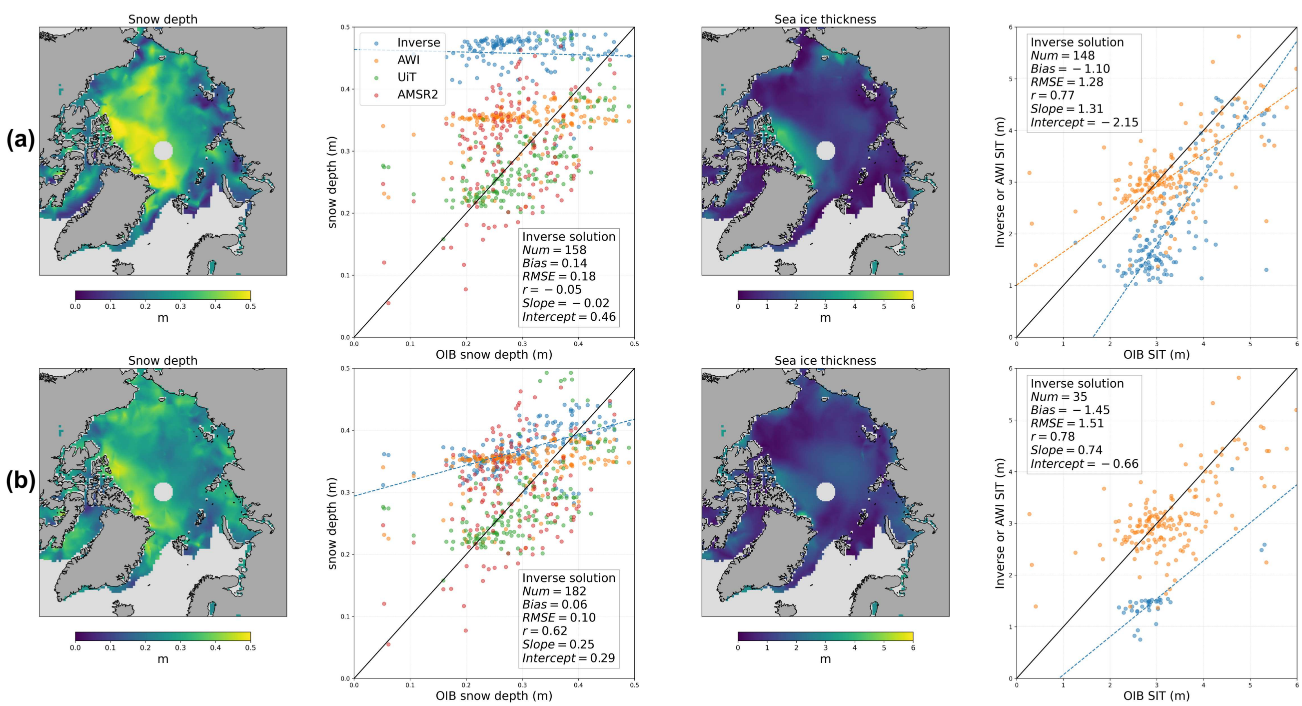

Figure S7. Comparison against OIB for (a) CS-IS-3p and (b) CS-IS-4p for April 2019. The comparison is made for (left column) SD and (right column) SIT.

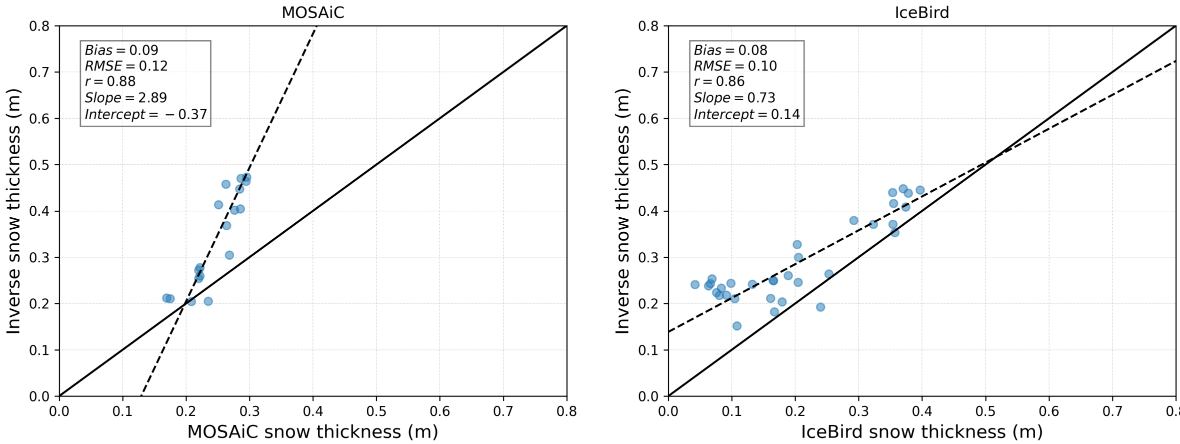

Figure S8. Evaluation of the results from the inversion using CS-IS-3p for SD. The validation is performed against MOSAiC (for Winter 2019-2020) and IceBird (for 2019/04).

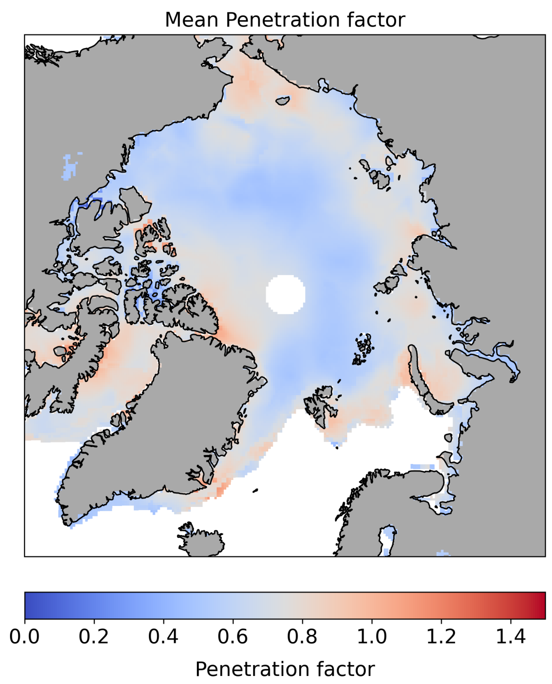

Figure S9. Mean bias factor computed with CS-IS-3p model for Winter 2019-2020.

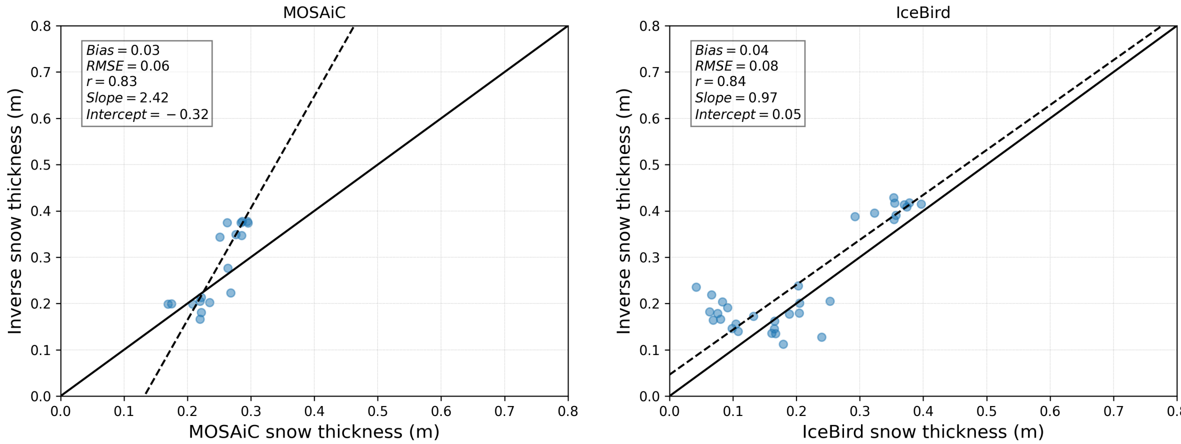

Figure S10. Evaluation of the results from the inversion using CS-IS-4p for SD. The validation is performed against MOSAiC (for Winter 2019-2020) and IceBird (for 2019/04).

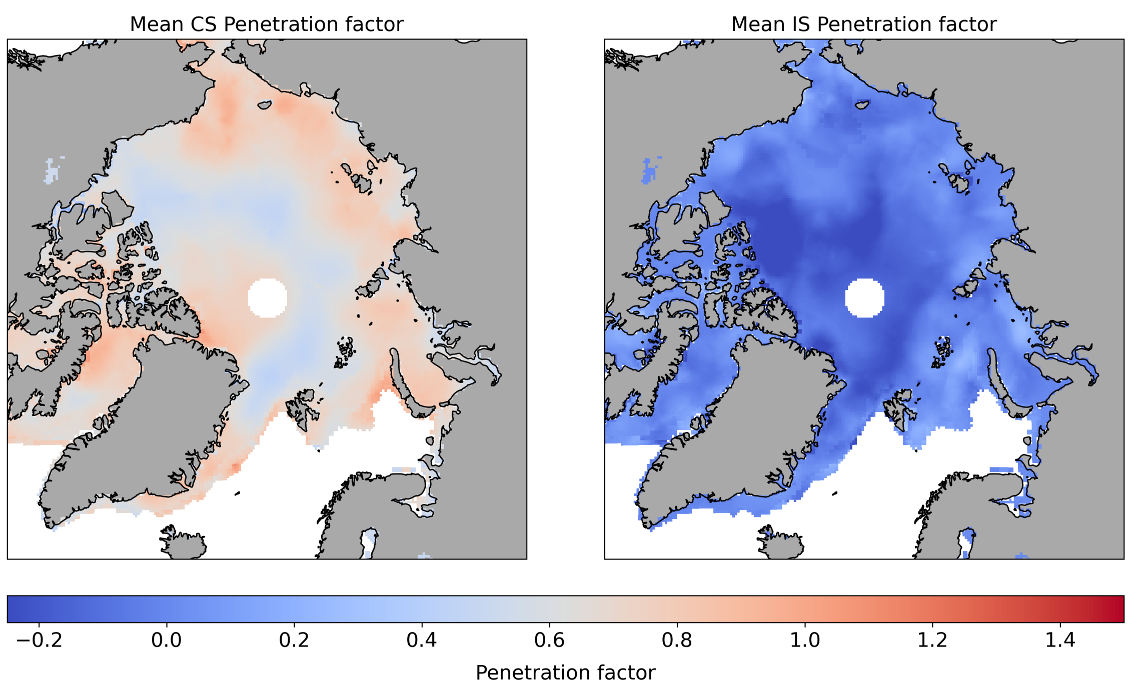

Figure S11. Average bias factors for (left) CryoSat-2 and (right) ICESat-2, for Winter 2019-2020, computed with CS-IS-4p.

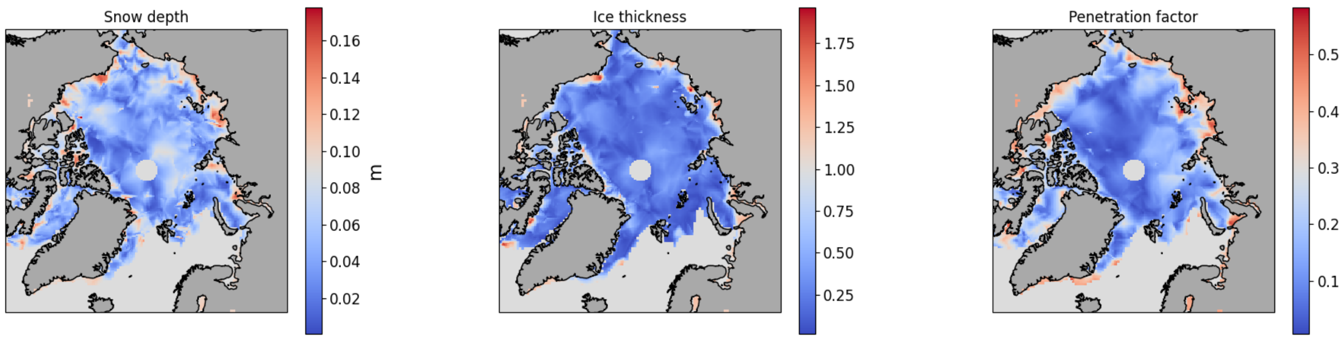

Figure S12. Standard deviations for the model CS-IS-3p for April 2019

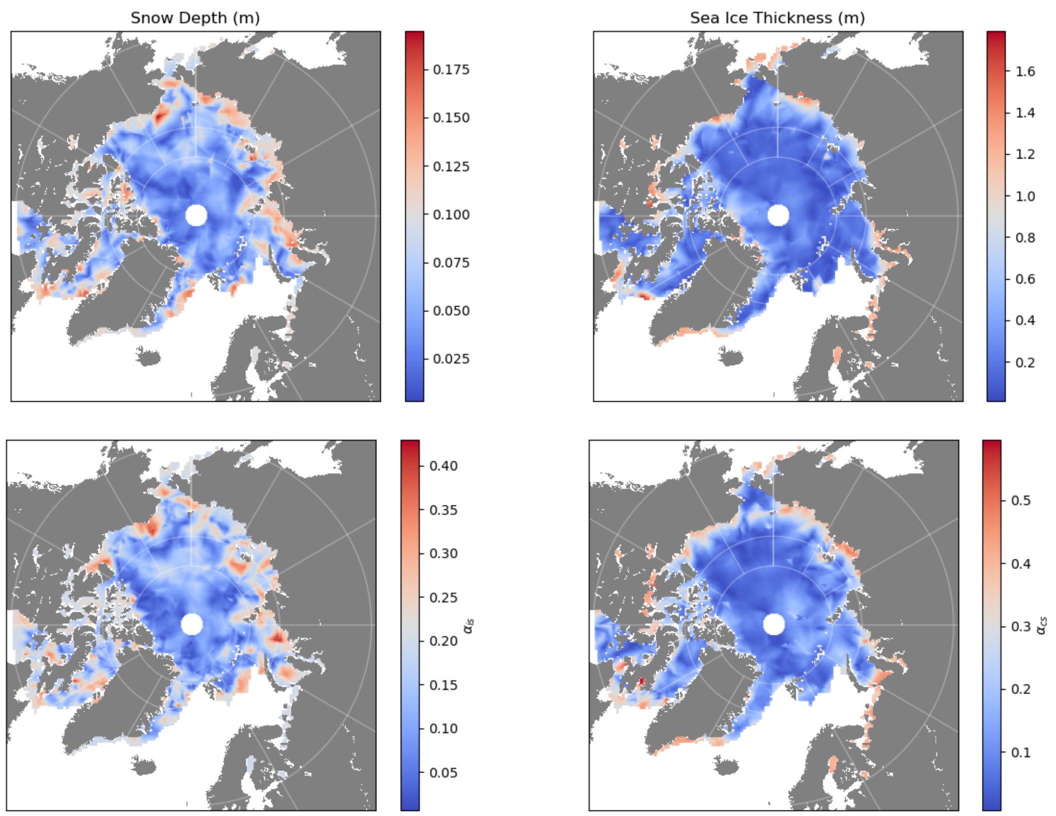

Figure S13. Standard deviations for the model CS-IS-4p for April 2019.

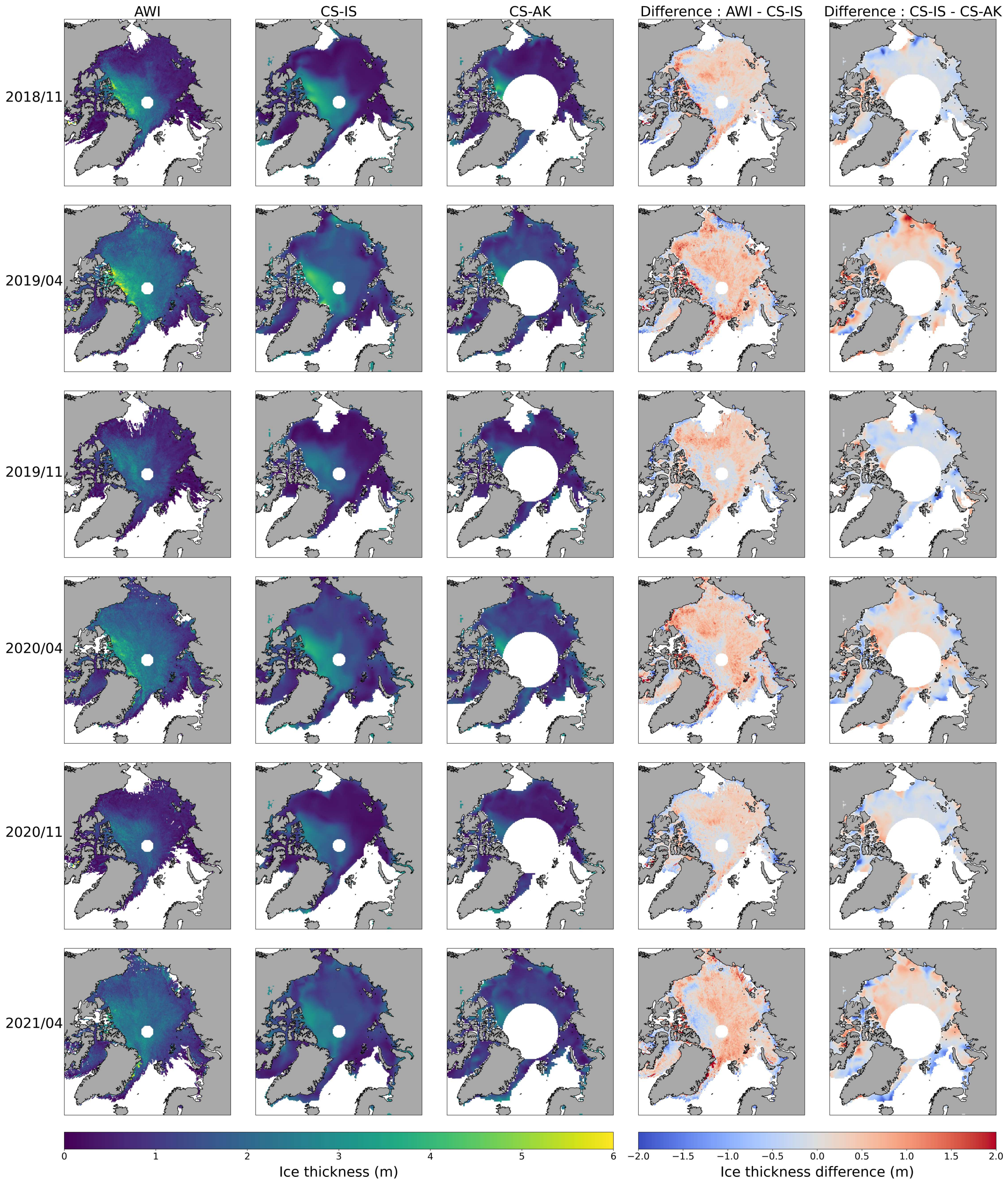

Figure S14. Same than Figure 1 (in the main paper) but with a constant 2 cm error for the input freeboards.

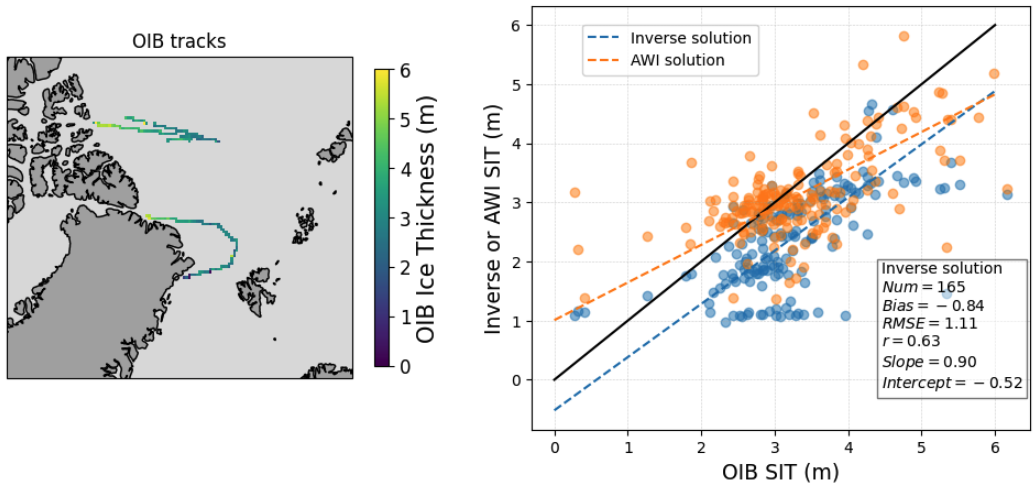

Figure S15. Comparison against OIB for SIT with CS-IS-2p-LARM and $\alpha_{cs} = 0.75$.

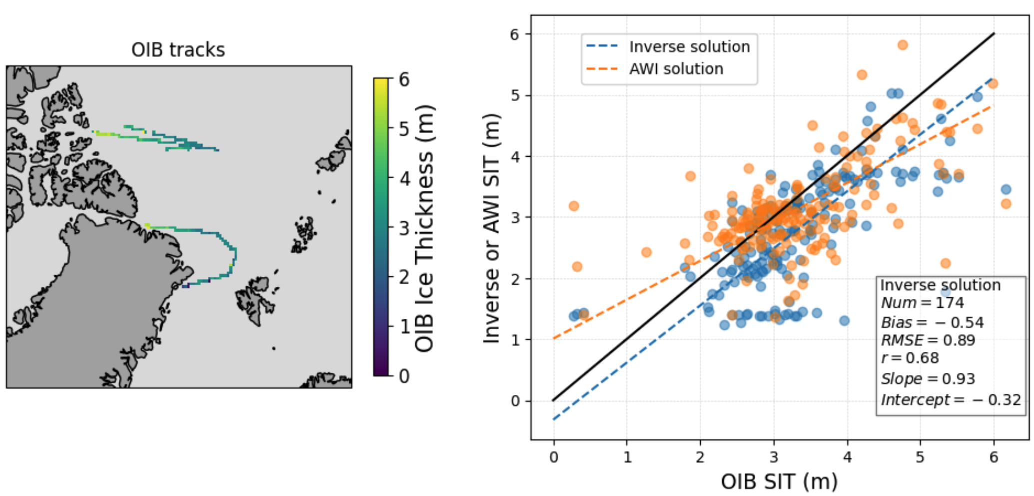

Figure S16. Comparison against OIB for SIT with CS-IS-2p-LARM and $\alpha_{cs} = 0.85$.

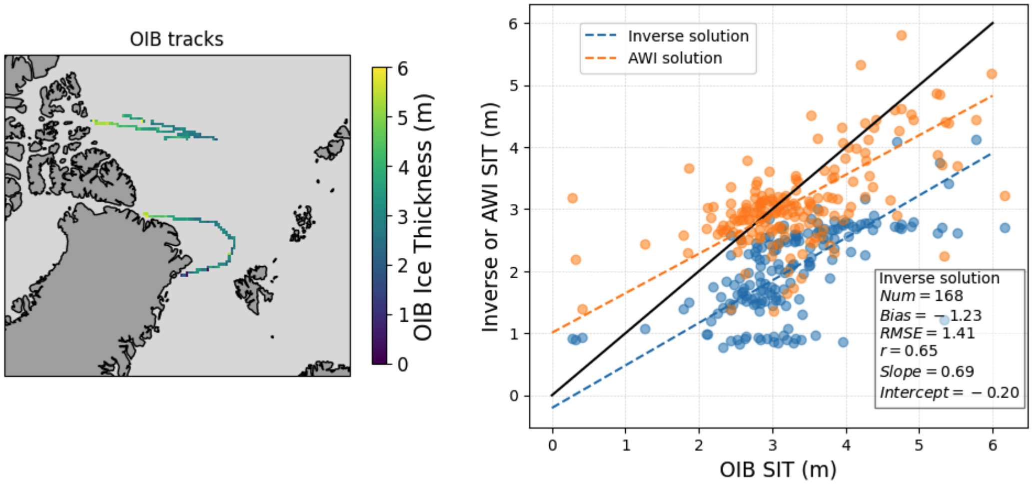

Figure S17. Comparison against OIB for SIT with CS-IS-2p-LARM and $\alpha_{cs} = 0.65$.

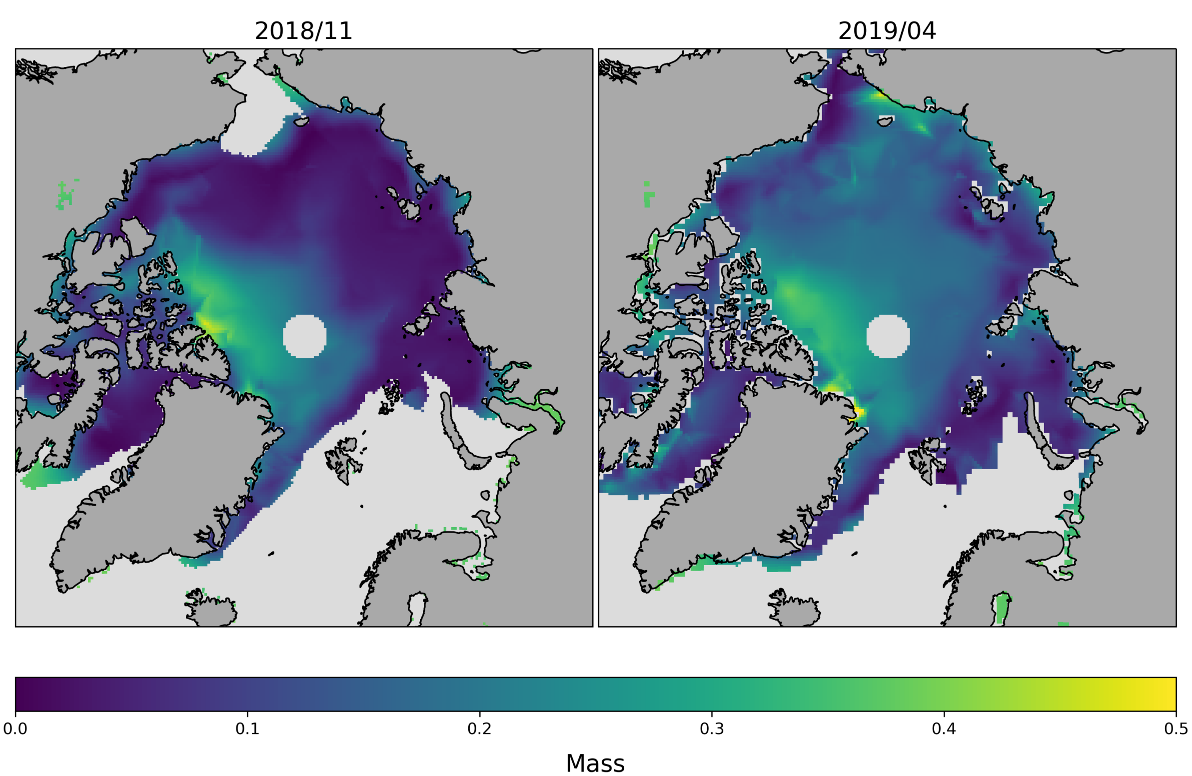

Figure S18. Inversion solution when inverting for the mass $\frac{\rho_w - \rho_i}{\rho_w} H_i$ for November 2018 and April 2019.